

Three-dimensional Numerical Model of Kerosene Evaporation in Gas Turbine Combustors

*Andrey A. Aksenov*¹ , *Sergey V. Zhluktov*¹ , *Vladimir S. Kashirin*¹ ,
*Marina L. Sazonova*¹ , *Sergey G. Cherny*² , *Ilia V. Zeziulin*³ ,
*Maria D. Kalugina*¹ 

© The Authors 2023. This paper is published with open access at SuperFri.org

A three-dimensional model of the multiphase flow based on the Eulerian–Eulerian approach was implemented using the FlowVision CFD package and, on this basis, a numerical algorithm for study of evaporation of liquid fuel was developed. The created high-performance complex for the carrier and dispersed phases interaction simulation was validated against the well-studied experimental problem of the evaporation and mixing of kerosene emerging from a flat pre-filming airblast atomizer for gas turbine combustors. In this work, the carrier phase is supposed to be air and kerosene vapors, and the dispersed phase is selected as liquid kerosene. Based on the calculated kerosene evaporation drops distributions, an important parameter that characterizes the spray fineness, Sauter mean diameter, is determined. Numerically calculated in the developed model the evaporation rate and Sauter mean diameter of fuel droplets agreed well with the experimental data. In famous works, the air temperature and pressure varied during the experiments. At the same time, in comparison with the calculated data, a stronger influence on the kerosene evaporation was obtained by air temperature than pressure. The dependence on pressure can be seen in the case of taking into account the corresponding changes in the liquid fuel properties. It is also noted that the initial fuel temperature is an important parameter for evaporation. This can be seen in the results of the kerosene evaporation numerical simulation carried out in this study.

Keywords: mathematical modeling, FlowVision, verification, dispersed phase, Eulerian–Eulerian approach, liquid fuel, droplets evaporation, Sauter mean diameter.

Introduction

1) *Numerical modeling is the most appropriate tool to study liquid fuel evaporation.* In gas turbine design, it is often necessary to develop devices for the atomization, evaporation, and mixing of liquid fuel within a given fuel droplet size range and uniformity of droplet distribution in the gas stream. At the same time, as a rule, a detailed experimental study of atomization and evaporation using real nozzles is difficult due to the wide range of particle sizes and the density of filling the gas stream with fuel particles. Therefore, the results of the evaporation and kerosene mixing detailed study under conditions similar to aircraft engines and stationary gas turbines demonstrated in [7] are of particular interest.

2) *The experimental data is for validation of numerical modeling.* One of the reasons for the experimental data given in [7] significance is their potential for validation (debugging, calibration, calculation methods development) of programs for fuel evaporation process numerical modeling. Numerical modeling is the most appropriate way (tools) to understand (comprehend) the flow structure and identify the factors that affect the fuel atomization and evaporation efficiency, and, therefore, the gas turbine energy conversion efficiency. For the evaluation of the mixing quality in the combustion chambers of aircraft and rocket engines, numerical modeling of the droplet jet formation is currently used to determine the fineness of atomization by the calculation of

¹“TESIS” LTD, Moscow, Russia

²Kutateladze Institute of Thermophysics of the Siberian Branch of the Russian Academy of Sciences, Novosibirsk, Russia

³Novosibirsk State University, Novosibirsk, Russia

Sauter mean diameter, taking into account primary and secondary decay, fusion and collision of droplets, which makes it possible to evaluate liquids atomization in a wide range of devices and modes. In turn, the correct evaluation of the fuel atomization is the fundament for a correct (detailed) description of its evaporation. This knowledge is very much in demand for device design. Therefore, at the stages of design, modernization, and optimization of these installations' operating modes, it is impossible to do without mathematical modeling of the processes occurring in these installations. The reliability of the results obtained in this case can only be guaranteed by the validation of the numerical model and its software implementation carried out on reliable experimental data. Validation of an analytical technique is experimental proof that the technique is suitable for solving the intended problems.

3) *FlowVision CFD is validated on experimental data.* In [7], a model of a pre-evaporator channel with full optical access operating at a pressure of up to 15 bar and a temperature of up to 850 K was created to conduct experiments on kerosene evaporation. During the experiment, the pressure, temperature, and airflow velocity, as well as the initial jet temperature and fuel consumption, were changed. It means there are unique data for the calibration of complex three-dimensional numerical models of kerosene atomization, evaporation, and mixing under conditions similar to aircraft engines and gas turbines. In this study, the FlowVision software package (FlowVision PC) is validated [3, 4] based on the unique experimental data from [7] in terms of the reliability of the results obtained on its basis for solving phase transition problems.

4) *Effective technique for numerical simulation fuel evaporation is of interest.* Even though a large number of works have been carried out on experimental and numerical studies of the processes of liquid evaporation in gas and the dependencies of the quality of gas, fuel and its evaporation products on the main parameters of fuel input have been compiled, interest in a more thorough study of the vaporization process is constantly increasing. New models are being developed, validated, and verified for both primary and secondary decay and droplet fusion, as well as evaporation and fuel combustion. The works considered below are the closest in terms of the studied processes and research methods. In [8], an effective technique for numerical simulation of a liquid jet decay in a compressed gas stream based on the Reynolds equations and the volume of fluid (VOF) method was developed. The technique describes the formation of primary droplets, and their transition to the Eulerian dispersed phase, where they undergo the secondary break-up and evaporation. In [11], Eulerian multicomponent model of liquid atomization and evaporation based on the WAVE decay model is presented. Special attention is paid to the modeling of thermal processes occurring inside moving droplets. A successful simulation of the dense liquid jets complex dynamic behavior has been carried out. In [9, 10], the large eddy simulation (LES) was used to describe the spray. In [9] a special attention is paid to the setting of turbulent boundary conditions. The comparison of the results obtained experimentally and numerically by the proposed model showed its good accuracy. A similar study was carried out in [10], which also investigated the effect of the mesh resolution on the spray global characteristics such as the penetration depth. In [12], direct numerical simulation (DNS) was applied to describe the sputtering of the flame of n-heptane in a vortex combustion chamber. Using the model, the contribution of the combustion of the preliminary mixture and the diffusion flame to the total heat release is estimated. Studies [13, 14] are devoted to the research of the fuel spray evolution in the engines combustion chambers. The CFD analysis carried out in [13] turned out to be the only chance to get a complete view on the fuel spray process, which made it possible to design the optimal geometry of the chamber. In [14], calculations were carried out for chambers

of various working volumes; it is noted that the simulation results show a good agreement with experimental data. Works by S. Tonini et al. [21, 22] are also devoted to modeling the spraying of dense diesel fuel compressed to high pressure – in [21] a description of the model, the approaches used, validation of the model is presented, and in [22] the influence of the number of fuel injections and the time between injections on the development of a cloud of droplets in the working chamber is studied. Several papers [18, 19] are devoted to the study of the flow parameters inside the nozzle influence on the fuel atomization in the working chamber. In [18], the effect of primary droplet decay on the characteristics of atomization and fuel combustion in diesel engines was studied. In particular, the KH-ACT model is considered, taking into account the contributions of cavitation and turbulence inside the nozzle to the droplets primary break-up. The results show improved agreement with the experiments in comparison with modeling using the KH model. In [19], the Eulerian model based on the VOF method and implemented in the CONVERGE CFD code was investigated. For the model, the influence of the nozzle outlet geometry on both the flow inside the nozzle and the further spray in the chamber is studied. The influence of the hole geometry on the droplets primary break-up of was established, which, in turn, affects further processes and characteristics, such as the fuel penetration depth into the working area, fuel evaporation, its mixing with air, and the spray fineness. A hybrid procedure for numerical simulation of two-phase flows in the combustion chamber is proposed in [17]. It is a two-stage combination of Eulerian and Lagrangian approaches. The Euler method gives a preliminary two-phase flow field. The Lagrangian method tracks the particle movement with a detailed description of the droplets secondary break-up. A 30% calculation of the spraying acceleration has been achieved compared to modeling based only on the Lagrangian method.

5) *The work is aimed at the fuel evaporation calculation and validation.* It should be noted that the works given in our brief review, as well as the works [3, 4], describe methods for calculating both atomization and evaporation of the dispersed phase. The FlowVision PC has a model of particle atomization during the secondary droplet decay and, in general, the secondary decay can be calculated in the package. However, the present work is aimed at the results of the fuel evaporation calculation validation. Therefore, the characteristics (parameters) of the fuel spray are taken from [7] for the calculation of the experimental setup [7]. At the same time, the possibility of varying the kerosene droplet diameter spectrum set at the chamber inlet is presented in the formulation of the problem. Analyzing the solution sensitivity to the spectrum, the range of changes in the diameters of kerosene droplets supplied to the chamber is selected, which ensures the evaporation rate and Sauter mean diameter of fuel droplets as much as possible coinciding with their values obtained experimentally. The proof of the FlowVision PC suitability for solving the vaporization of the dispersed phase problem is relevant for numerical studies presented in [3, 4] since the correctness of the carbon black production reactor operation evaluation obtained in these works significantly depends on this.

6) *The article is organized as follows.* Section 1 is described a problem statement as experimental setup and assumptions that we used for mathematical model. Section 2 contains description of mathematical model into FlowVision CFD. That model contains continues and dispersed phased that are described by different set of equations. In section 3 we showing results of numerical modeling in comparison of physical experiment. Several hypotheses were tested in additional to the comparison of mathematical model and experiment. Conclusion summarizes the study and results from section 3.

1. Problem Statement

1.1. Experimental Setup

The experimental setup from [7] is shown in Fig. 1. The experimental setup working section is a rectangular duct with a cross-section of 25 mm × 40 mm and an observable streamwise pathlength of about 180 mm. To prevent overheating of the pressure housing, the quartz glass duct was surrounded by a cooling airflow. At a given temperature of the main air, the pressure inside the duct was regulated by changing the air flux and using throttles of different diameters at the duct outlet.

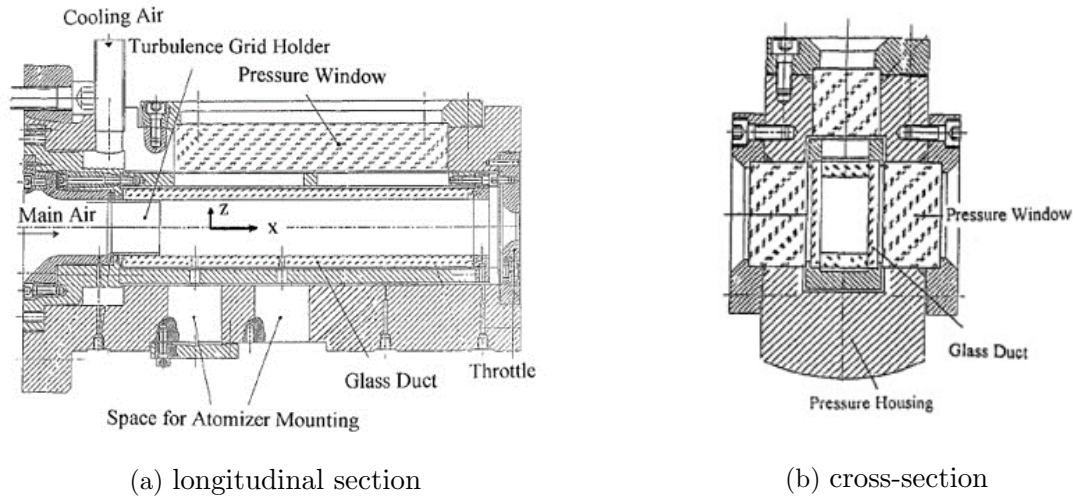


Figure 1. The experimental setup [7]

The setup allows to install a liquid fuel atomizer inside the channel in two axial positions. The atomizer shape is shown in Fig. 2. There was used an atomizer with a flat film section. The film was atomized by a high-speed incoming airflow. The atomizer width is 8 mm, the slit height is 0.1 mm. The atomizer material is stainless steel. The atomizer film section coincides with the horizontal symmetry plane of the duct XY. The origin of the coordinate system is located in the middle of the atomizer edge. To measure the fuel temperature, a thermocouple was installed on the atomizer film section surface. To protect against the atomizer housing thermal conductivity, the thermocouple was insulated with a ceramic bond. More than 70% of the sensor volume was located in the insulator so that the film flow on the atomizer surface was not disturbed by the sensor.

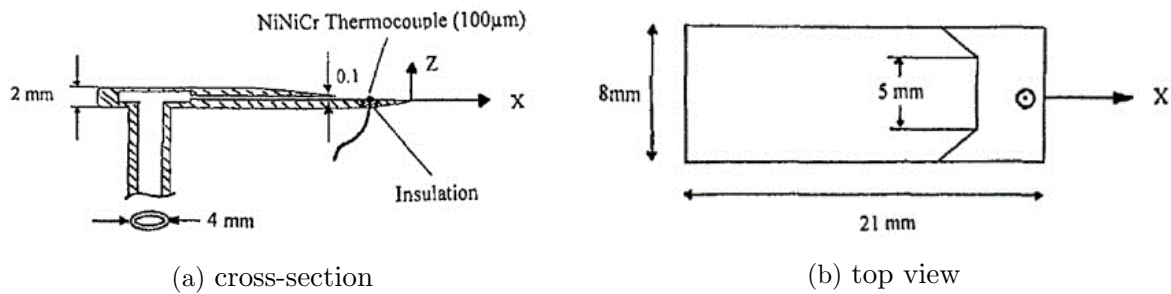


Figure 2. The airblast atomizer

Jet A1 kerosene, whose physical properties are of kerosene itself and its vapors, presented in [15], was used as a liquid fuel during the experiment. The parameters of the experimental mode, defined as the basic ones for numerical simulation, are given in Tab. 1.

Table 1. Experimental mode parameters defined as the basic for the numerical simulation

Physical property	Value
Air pressure	9 bar
Air temperature	750 K
Air speed (ratio of volumetric airflow to duct cross-sectional area)	120 m/s
Liquid fuel temperature (measured on the atomizer surface)	453 K
Fuel mass flow	1 g/s (125 g/s/m per unit length of the atomizer edge)

The control sections of the computational domain at which the flow characteristics are analyzed are located at distances from the sprayer $x = 30$ mm, 60 mm, 100 mm, 150 mm. The computational domain is sectioned and flow characteristics are analyzed at distances of $x = 30$ mm, 60 mm, 100 mm, 150 mm from the sprayer. The fuel evaporation rate V_{evap}/V_0 (the ratio of the difference in the fuel droplets volume flows in the input section x_0 and control sections x_k to the flow in x_0) and droplets Sauter mean diameter are taken as control flow characteristics (hereinafter referred to as “control parameters”).

1.2. Numerical Model Assumptions

As noted in the introduction, atomization of the film is not considered in the computational model. A discrete distribution of droplet diameters by size – a droplet size spectrum – is set at the chamber inlet (the atomizer exit). The fuel inlet is established as the zero x-coordinate (atomizer edge), though according to experimental materials it is noted that the film primary atomization is completed at the distance of 10 mm from the atomizer. The velocity of the dispersed phase (droplets) V_d at the fuel inlet is assumed to be 10 m/s based on the calculation data in [7]. The fuel phase volume fraction at the inlet is determined by taking into account the selected speed and the experimental mass flow rate (Tab. 1). The distribution function $\frac{dQ}{dD}$ of the volume occupied by droplets with diameter D and normalized to its maximum value $\frac{dQ}{dD}$ is taken from the results of the “cold” experiment in [7]. This distribution function is shown in Fig. 3 as a solid line, and its values are shown on the right.

According to the given curve, a discrete distribution of the droplet volume fraction ϕ is calculated. To do this, N_d (the number of droplets with a diameter d_i in the diameter spectrum) is determined, for which the value $\frac{dQ}{dD}(d_i)$ is calculated. After that, the volume fraction ϕ_i of droplets with a diameter d_i in the dispersed phase is calculated

$$\phi_i = \frac{\frac{dQ}{dD}(d_i)}{\sum_{i=1}^{N_d} \frac{dQ}{dD}(d_i)}. \quad (1)$$

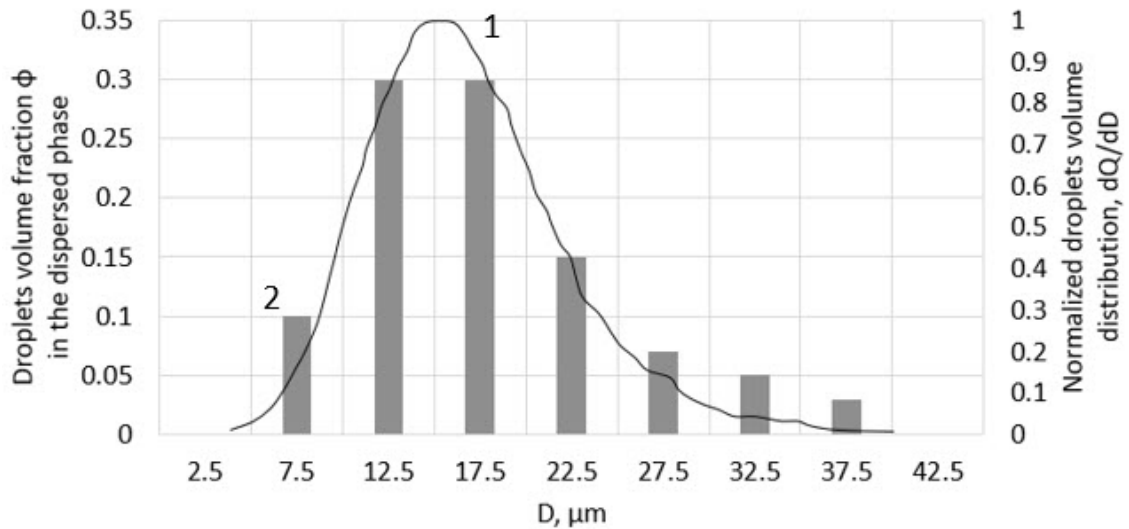


Figure 3. Droplets diameter spectrum at the chamber entrance: 1 – diameter distribution function obtained in the “cold” experiment [7], 2 – selected for FlowVision calculation values

Expression (1) ensures the fulfillment of the condition $\sum_{i=1}^{N_d} \phi_i = 1$. Volume fraction values and the corresponding droplet diameters of the fuel droplet size spectrum at the inlet, taken as the basic, are shown in Tab. 2. Also, a histogram in Fig. 3 shows the discrete droplet diameter distribution, which was selected for calculation in FlowVision, these values are shown on the left. At the fuel (dispersed phase) inlet, its volume fraction α is set. At a given kerosene velocity at the atomizer exit (fuel inlet) $V_d = 10$ m/s, the volume fraction α is calculated from experimental data (Tab. 1) as

$$\alpha = \frac{Q_d}{\rho(T_d) \cdot V_d \cdot S},$$

where Q_d is the kerosene mass flux, S is the atomizer exit area. The droplet concentration value for each family (set) $n_{d,i}$ at the fuel inlet is determined for the concentration equation by α , as well as by the distribution ϕ_i depending on d_i :

$$n_{d,i} = \alpha \cdot \frac{\phi_i(d_i)}{V(d_i)}. \quad (2)$$

Here $V(d_i)$ is the drop of diameter d_i volume. It is assumed in this model that all drops are balls of diameter d_i . The equations given in paragraphs 2.1–2.2 are solved separately for each particles family i . It should be noted that in the case of solving this problem based on the Eulerian–Lagrangian approach, the number of fuel droplets N_i passed through the atomizer exit per unit of time in each family (set) corresponding to the current diameter d_i of a given fuel droplet size spectrum may be calculated from (2) as

$$\frac{dN_i}{dt} = n_i \cdot V_d \cdot S = \alpha \cdot \frac{\phi_i(d_i)}{V(d_i)} \cdot V_d \cdot S. \quad (3)$$

The inlet gas velocity is selected based on preliminary calculations of the carrier phase without taking into account the dispersed phase results at a distance of 10 mm from the atomizer near its film section level. Due to the lack of experimental data on the effect on the problem solution changes of:

Table 2. Droplet diameter spectrum at the chamber entrance

Family number, i	1	2	3	4	5	6	7
Family particle diameter d_i , μm	7.5	12.5	17.5	22.5	27.5	32.5	37.5
Family volume fraction in the dispersed phase ϕ_i	0.1	0.3	0.3	0.15	0.07	0.05	0.03

- fuel velocity in the flow after the film is torn off the edge of the atomizer;
- droplet size distribution (diameter) after the film atomization;
- degree of turbulence in the incoming airflow;

the accepted assumptions are verified in this study by investigation of the sensitivity of the problem solution to change:

- droplet velocity at the fuel inlet;
- droplet size range at the fuel inlet;
- turbulence parameters at the air inlet.

2. Mathematical Model

The study of the liquid fuel evaporation is carried out in the FlowVision software package [1–4]. The evaporation of fuel droplets in the air stream is modeled using the Eulerian approach to describe the interaction between the continuous (carrier) and dispersed phase [20]. The following physical processes are modeled in the continuous phase: motion, turbulence, heat transfer, mass transfer; in the dispersed phase – motion, mass transfer, heat transfer. A detailed description of the mathematical model is given in [3], this paper only provides the short form of the main equations used in obtaining the problem solution.

2.1. Continuous Phase

The equations for continuity and momentum conservation in a continuous medium are

$$\frac{\partial(\phi_c \rho_c)}{\partial t} + \nabla \cdot (\phi_c \rho_c \mathbf{V}_c) = Q_d^{mass},$$

$$\frac{\partial(\phi_c \rho_c \mathbf{V}_c)}{\partial t} + \nabla \cdot (\phi_c \rho_c \mathbf{V}_c \cdot \mathbf{V}_c) = -\phi_c \nabla p + \nabla \cdot (\phi_c \hat{\tau}_{\text{eff}}).$$

Here ϕ_c , ρ_c , \mathbf{V}_c , p are the volume fraction, the density, the velocity, and the pressure of the continuous phase, Q_d^{mass} is the source term, n_d and M_d are the dispersed phase particle concentration and mass, τ_{eff} is the effective viscous stress tensor, which depends on the continuous phase dynamic coefficient of molecular and turbulent viscosities. Turbulence is described using the KEFV model [3, 5, 20–23]. The dispersed phase influences the carrier phase through the terms on the right-hand side of the Navier–Stokes equations describing the motion of the carrier phase (coolant gas). The equation for the energy balance of a continuous phase, written with respect to the total enthalpy H_c , has the form

$$\frac{\partial(\phi_c \rho_c \mathbf{H}_c)}{\partial t} + \nabla \cdot (\phi_c \rho_c \mathbf{V}_c H_c) = \frac{\partial(\phi_c P)}{\partial t} - \nabla \cdot (\phi_c \mathbf{J}_q) + \phi_c Q_{vis,G} - Q_d^{enth}.$$

Here \mathbf{J}_q is the effective enthalpy diffusion flux, $Q_{vis,G}$ and Q_d^{enth} are source terms. The mass fraction of the evaporated raw material is determined from

$$\frac{\partial(\phi_c \rho_c Y_i)}{\partial t} + \nabla \cdot (\phi_c \rho_c Y_i \mathbf{V}) = -\nabla \cdot (\phi_c \mathbf{J}_{i,\text{eff}}) + Q_{d,i}^{mass},$$

$$\mathbf{J}_{i,\text{eff}} = -(\rho D_i + \frac{\mu_t}{Sc_t}) \nabla Y_i = -(\frac{\mu_t}{Sc_i} + \frac{\mu_t}{Sc_t}) \nabla Y_i,$$

where Y_i and $\mathbf{J}_{i,\text{eff}}$ are the continuous phase mass fraction and the effective diffusion flux of the i -th substance, $Q_{d,i}^{mass}$ is the continuous phase i -th substance mass source due to dispersed phase mass change (if the dispersed phase consists of one substance, then $Q_{d,i}^{mass} = Q_d^{mass}$), $Sc_i = \frac{\mu}{\rho_c D_i}$ and $Sc_t = \frac{\mu_t}{\rho_c D_t}$ are the molecular and turbulent Schmidt numbers and D_i is the continuous phase diffusion coefficient of the i -th substance. The evaporated raw materials are added to the heat carrier gas, forming the carrier phase.

2.2. Dispersed Phase

2.2.1. Approaches to modeling evaporation/condensation of particles (droplets)

Evaporation/condensation processes of particles on a surface are described by the particle mass transfer equation for variable $M_d n_d$:

$$\frac{\partial(M_d n_d)}{\partial t} + \nabla \cdot (\mathbf{V}_d M_d n_d) = \nabla \cdot (\frac{\nu_{t,d}}{Sc_{t,d}} \nabla(M_d n_d)) - Q_d^{mass} + M_d \dot{n}_d.$$

The values of particle concentration n_d^n , n_d^{n+1} on two adjacent layers in time are assumed to be known during the equation integration. The source member Q_d^{mass} is figured out as

$$Q_d^{mass} = n_d \pi d^2 \dot{m}_d = n_d \pi d^2 \sum_{i=1}^{N_d} \dot{m}_{d,i}.$$

Here \dot{m}_d is the specific rate of the particle phase mass change, $\dot{m}_{d,i}$ is the specific rate of i -th substance of the particle phase mass change, N_d is the number of the dispersed phase substances, d is the particle diameter.

2.2.2. Particle mass, momentum, and energy conservation equations

The particles transport is described by the inhomogeneous convective-diffusion equation for the particles concentration:

$$\frac{\partial(n_d)}{\partial t} + \nabla \cdot (\mathbf{V}_d n_d) = \nabla \cdot (\frac{\nu_{t,d}}{Sc_{t,d}} \nabla n_d) + \dot{n}_d,$$

$$\nu_{t,d} = \nu_{t,c},$$

where \mathbf{V}_d is the dispersed phase (particles) velocity, $\nu_{t,d}$ and $\nu_{t,c}$ are the dispersed and continuous phase kinematic coefficients of the turbulent viscosity and $Sc_{t,d}$ – turbulent Schmidt number. The velocity of the dispersed phase (particles) in the main flow \mathbf{V}_d is determined by the particle momentum transfer equation, which is a non-uniform convective-diffusion equation for the conservative variable $\mathbf{V}_d M_d n_d$:

$$\frac{\partial(\mathbf{V}_{d,i} M_d n_d)}{\partial t} + \nabla \cdot (\mathbf{V}_d \mathbf{V}_{d,i} M_d n_d) = \nabla \cdot (\frac{\nu_{t,d}}{Sc_{t,d}} \nabla(\mathbf{V}_{d,i} M_d n_d)) - n_d \frac{\pi d^3}{6} \nabla_i p + F_{D,i}.$$

The force \mathbf{F}_D should be understood as the total force acting on the particle. It is obtained from the addition of repulsive, lift and drag forces. The values of the particle concentration n_d^n , n_d^{n+1} and their masses M_d^n , M_d^{n+1} on two adjacent layers in time are assumed to be known during the equation integration. The dispersed phase energy transfer is described by an inhomogeneous convective-diffusion equation for the conservative variable $h_d M_d n_d$:

$$\frac{\partial(h_d M_d n_d)}{\partial t} + \nabla \cdot (\mathbf{V}_d h_d M_d n_d) = \nabla \cdot (\frac{\nu_{t,d}}{Sc_{t,d}} \nabla(h_d M_d n_d)) + Q_d^{enth},$$

where h_d is the thermodynamic enthalpy of the particle phase.

3. Results and Discussion

3.1. Model Calibration under the Basic Mode Conditions

3.1.1. Computational grid

Grid convergence studies were performed for a 2D formulation of the problem. In this case, the central cross-section of the rectangular chamber was selected as the computational domain. The shape of the atomizer cross-section was modeled as illustrated in Fig. 4.

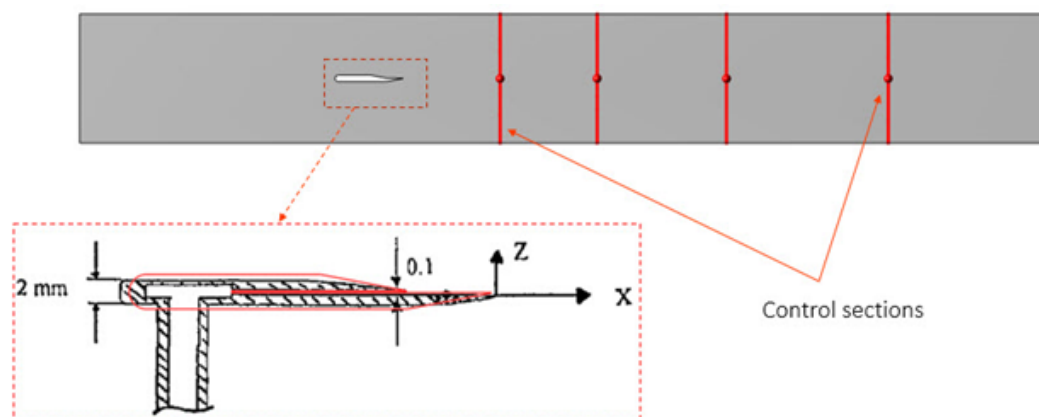


Figure 4. The computational domain with a schematized atomizer in the two-dimensional problem formulation

The initial mesh was generated with a uniform characteristic cell size of about 1.25 mm. Next, mesh adaptation of the computational domain volume was applied near the atomizer inlet and channel walls. In the FlowVision software, one level of adaptation involves dividing a Cartesian cell into 8 equal ones. As the computational domain was refined, the pressure drop change in the channel was monitored. As a result of the grid convergence studies, the third level of adaptation was chosen to be used near atomizer and channel walls. Selecting the fourth level of adaptation gives about a 3% change in the control parameter. The average Y^+ value was about 50. The single-phase flow of air alone is firstly considered under the conditions specified in Table 1 on the grid constructed as mentioned below. The turbulence intensity at the channel entrance was set to 3%, and the turbulence scale was 2.5 mm. In the simulation of single-phase flow, the air velocity obtained at a distance of 10 mm from the atomizer, near its film section, was 106 m/s. This value was set as the gas boundary condition in the fuel inlet section for the grid design refinement taking into account the dispersed phase. At the same kerosene inlet, the volume fraction of the dispersed phase was set equal to 0.1844, which provides the required fuel consumption when its velocity equals 10 m/s. In two-phase calculations of the gas-plus-kerosene system, additional adaptation of the computational mesh was applied behind the atomizer. The level of additional adaptation was based on a condition of dispersed phase volume fraction – only regions where the dispersed phase volume fraction had values in the range 10^{-10} to 1 were adapted. Figure 5 shows the profiles of the liquid-fuel volume fraction and the mass fraction of its vapors, obtained at different adaptation levels in the control section furthest from the atomizer, at $x = 150$ mm.

The third level of the adaptation with the dispersed phase volume condition was selected for use in further calculations. The cell count was 150.4 thousand. The resulting grid, which was used in calculations, is shown in Fig. 6.

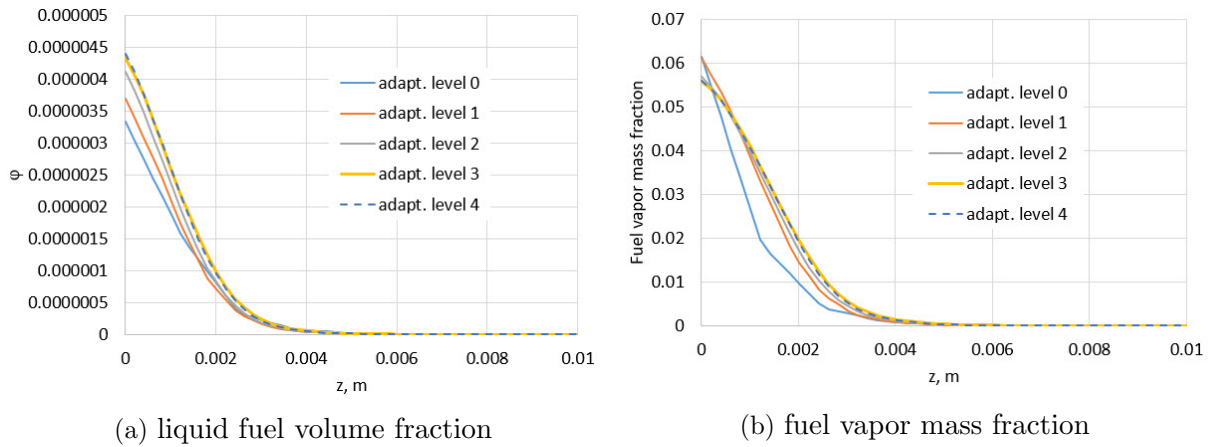


Figure 5. Dependence on the grid adaptation levels of the fuel (a) and vapor (b) distributions in the cross-section $x = 150$ mm along the duct length from the center line

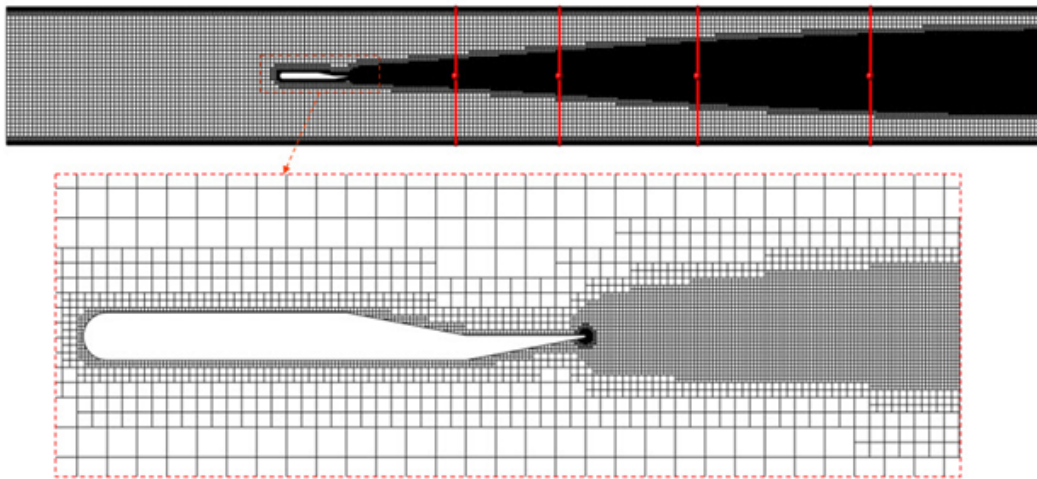


Figure 6. A grid for a two-dimensional formulation based on the results of the numerical solution convergence study

The calculated values of the control parameters – kerosene evaporation rate and Sauter mean diameter of fuel droplets are shown in Fig. 7 in comparison with the experimental data for the basic mode (Tab. 1).

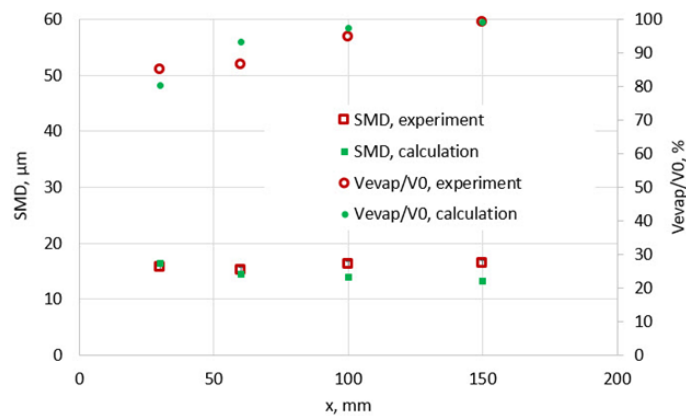


Figure 7. Fuel droplets evaporation rate and Sauter mean diameter in basic calculation mode

3.1.2. Assessment of the influence of atomizer shape

Due to the lack of precise dimensions parameters of the atomizer used in the experiments, taking into account the accepted method of the fuel supply (droplets form from the atomizer edge), the transition to a simplified atomizer model with a rectangular cross-section, which sizes are equal to the atomizer length and the kerosene supply gap size (Fig. 8), is considered. The negligible change in the control parameters as a result of calculations with a simplified geometry indicates a weak influence of its shape on the solution in the given formulation. Subsequent calculations model the atomizer with a rectangular cross-section (simplified geometry).

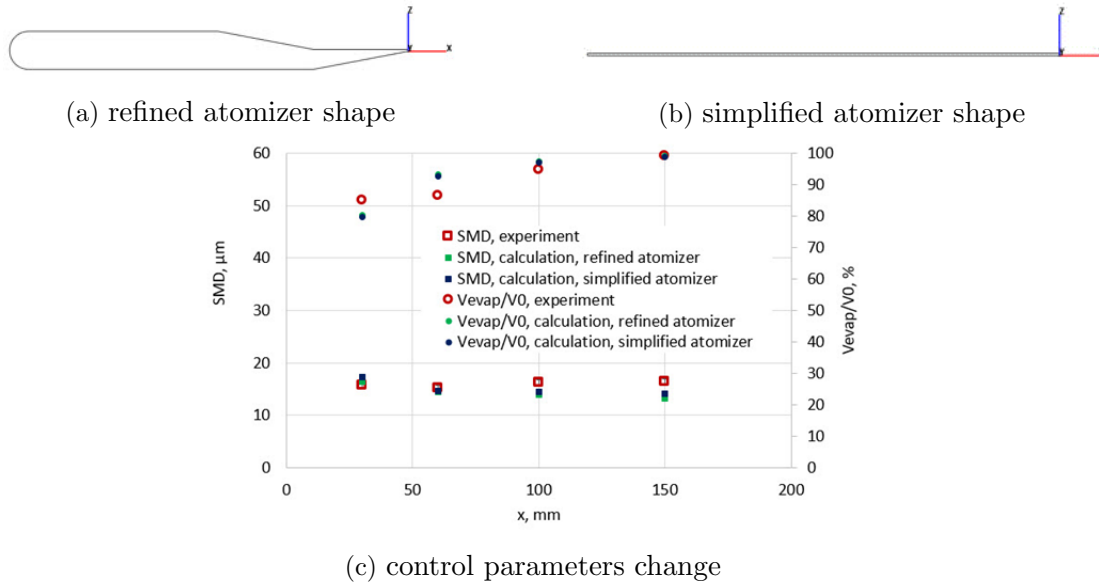


Figure 8. Assessment of the influence of atomizer shape

3.1.3. Assessment of the influence of droplet inlet velocity

Two types of fuel inlet boundary conditions were considered:

- inlet droplets velocity 10 m/s, dispersed phase volume fraction 0.1844, air velocity 106 m/s (droplet velocity values based on calculations in [7]);
- inlet droplets velocity 1.844 m/s, dispersed phase volume fraction 1, air velocity 0 m/s (droplet velocity values based on the experimental fuel flow rate).

The respective calculation results are shown in Fig. 9. These results indicate that determining kerosene inlet velocity from its flow rate is both acceptable and justifiable.

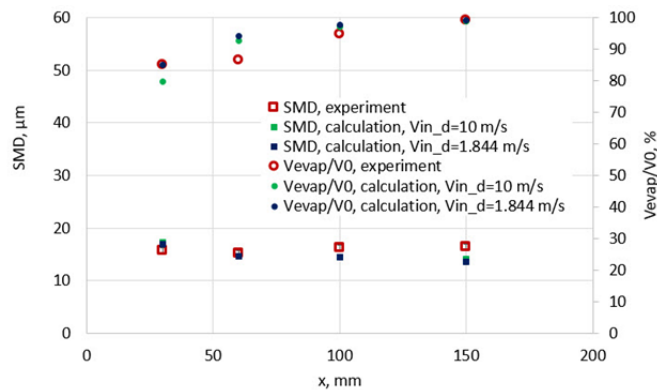


Figure 9. Assessment of the influence of droplet inlet velocity

3.1.4. Assessment of the influence of the spectrum of inlet fuel droplets

As observed in the calculation results presented above, the deviation of the droplet Sauter mean diameter from experimental values increases in control sections located further away from the atomizer. To identify the source of the deviation of this control parameters calculated values from experimentally obtained ones, the computational model solution sensitivity analysis to the spectrum of kerosene droplet diameters, which are set as inlet parameter, was carried out. The basic spectrum of fuel droplet diameters was obtained from the results of the cold experiments [7]. The considered spectrum variations, which were obtained by changing the values of the largest particle group volume fractions in the dispersed phase at the fuel inlet, are shown in Tab. 3. The basic spectrum corresponds to the set of droplets denoted D1.

Table 3. Variations of the particle diameter spectrum at the inlet

Particle group diameter D, μm	Spectrum				
	D1	D2	D3	D4	D5
Particle group volume fraction ϕ					
2.5	0	0	0.03	0	0
7.5	0.1	0.1	0.1	0.07	0.1
12.5	0.3	0.3	0.3	0.3	0.3
17.5	0.3	0.3	0.3	0.3	0.3
22.5	0.15	0.15	0.15	0.15	0.15
27.5	0.07	0.07	0.07	0.07	0.07
32.5	0.05	0.05	0.05	0.06	0.05
37.5	0.03	0.01	0	0.05	0.01
40	0	0	0	0	0.01
45	0	0	0	0	0.01
50	0	0.01	0	0	0
60	0	0.01	0	0	0

A comparison of the control parameters calculated for the spectra of Tab. 3 is shown in Fig. 10. The spectrum of fuel droplet sizes at the input has the greatest influence on the solution out of all the considered modeled input parameters, ambiguously determined from [7]. The closest match of SMD control cross-sections to experimental data was obtained with the D5 spectrum. Subsequent studies were carried out using the inlet kerosene droplet diameter spectrum denoted D5 in Tab. 3.

3.1.5. Assessment of jet spray width

According to the experimental data in [7], the control sections are given a value Z0.9, defined as the half-width of the profile which contains 90% of the measured volumetric fuel flow rate (liquid and vapor). The factors affecting the spray width of the jet are the following:

- gas turbulence [7, 16];
- fuel droplets, which are tearing off atomizer edge, fluctuations [7, 16];
- main stream velocity fluctuations [6].

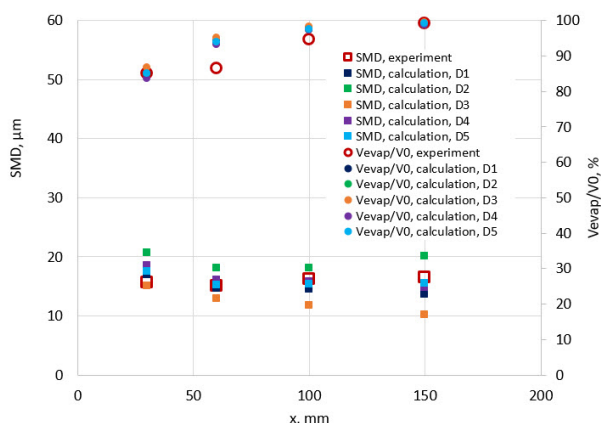


Figure 10. Droplets inlet size spectrum change estimation

To study the effect on the jet spray width in the computational model, it was opted to alter the parameter of inlet air turbulence. Figure 11 shows the magnitude of Z0.9 values obtained from calculations using different values of pulsations and turbulence scales in the air flow at the channel entrance.

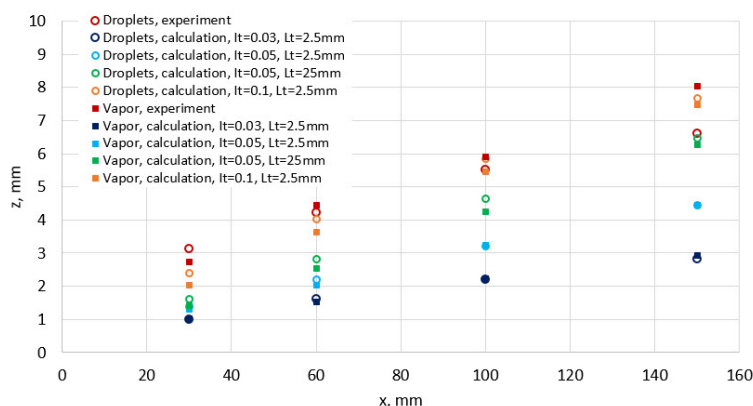


Figure 11. The half-width of the profile, which contains 90% of the measured volumetric fuel consumption (liquid and vapor)

Increasing the incoming flow pulsations from 3% to 10% achieves an up to $2\times$ increase in profile width, which contains 90% of the measured volumetric fuel consumption, thus matching the experimentally measured values. At the same time, the change in the control characteristics of evaporation rate and droplet Sauter mean diameter is negligible. Figure 12 shows changes in the kerosene vapors mass fraction distribution as a result of an increase in the airflow turbulence intensity at the inlet.

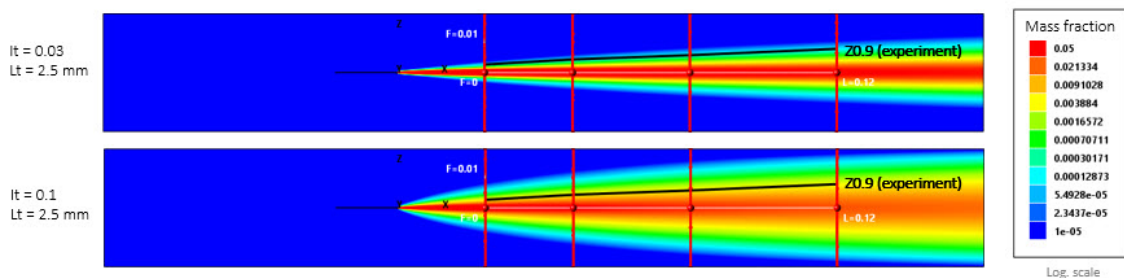


Figure 12. Kerosene vapors mass fraction distribution for different airflow turbulence parameters

3.2. Model Analysis under Different Experimental Conditions

3.2.1. Influence of airflow temperature regime and pressure

In the basic experimental scenario, the air temperature is equal to 750 K and pressure is 9 bar in the duct setup. [7] presents results with these parameters changed to the following values:

- air temperature 650 K, 850K;
- air pressure 6 bar, 12 bar.

Numerical simulations with these conditions were performed using the computational model constructed in the FlowVision CFD package. Simulations were performed with a simple change in air temperature and pressure, but also with an adjustment of fuel parameters to account for the change in its properties under the new conditions. Airflow under different temperature regime interactions leads to a change in fuel temperature on the atomizer surface. Values measured with a thermocouple under different experimental conditions are given in [6]. The corresponding correction of the liquid kerosene thermophysical properties (in particular, its surface tension) determines the change in its dispersed composition after the film spraying. In order to confirm the droplet diameter size distribution, which was accepted as an input parameter from the cold experiment (paragraph 2.1) based on the [7], the droplet size diameter adjustment is defined as

$$D_{new} = k \cdot D_{ini},$$

$$k = \frac{\left(\frac{\sigma_{fuel}}{\rho_{air}^{0.3}}\right)_{new}}{\left(\frac{\sigma_{fuel}}{\rho_{air}^{0.3}}\right)_{ini}},$$

where D_{new} is the new diameter value, D_{ini} is the original diameter value, σ_{fuel} is the liquid fuel surface tension, and ρ_{air} is the air density. The results of control parameters (the evaporation rate and droplet Sauter mean diameter) calculations under another set of experimental conditions are shown in Fig. 13.

The calculation results approach the experimental data by adjusting the input data for fuel droplets, taking into account changes in air pressure and temperature. However, the chosen method of the correction probably does not accurately describe real conditions (in particular, the droplet size spectrum), which is the reason for the observed deviations in the control parameter values.

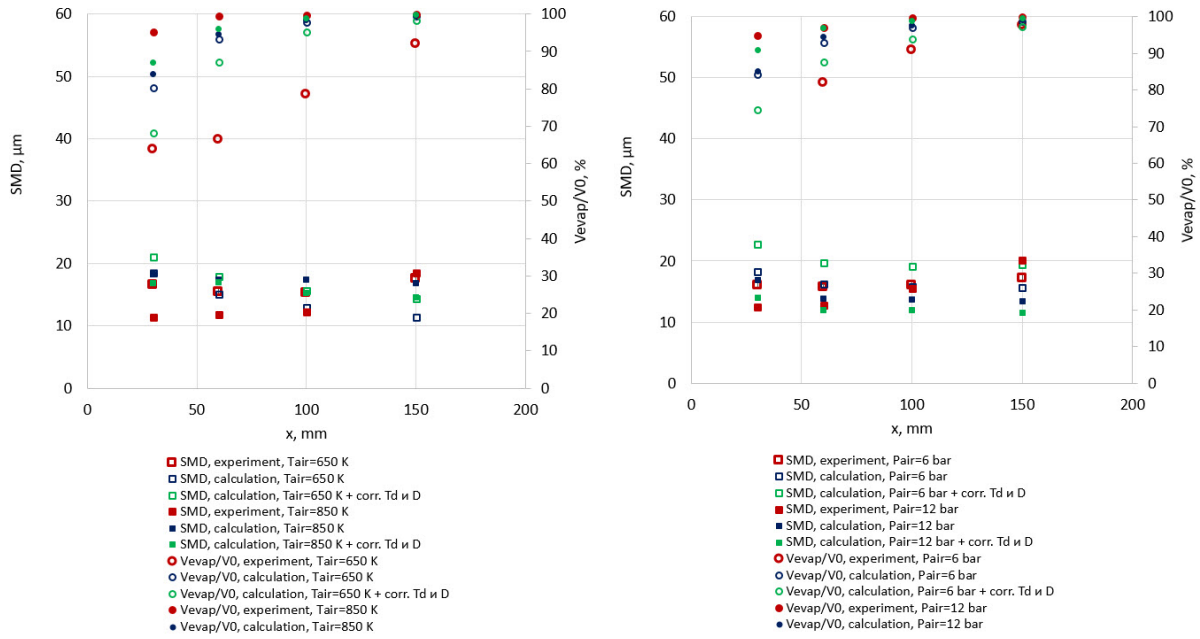
3.2.2. Influence of the dimensionality in the problem statement

The study of kerosene evaporation in the premix duct for a gas turbines combustion chamber at high pressure is also considered as a three-dimensional formulation within the scope of this work. The parameters of the derived two-dimensional model were transferred to a three-dimensional formulation for the rectangular duct. The atomizer shape was modeled as the simplified one obtained as a result of studies carried out in paragraph 3.1.2. Figure 14 shows the isometry of the spatial computational domain and boundary conditions.

FlowVision provides the following options for boundary conditions of dispersed phase particles near solid walls.

Particles can:

- bounce elastically off the wall;
- bounce inelastically;
- stick to it.



(a) air temperature: 650 K, 850 K

(b) air pressure: 6 bar, 12 bar

Figure 13. Calculation results for another set of experimental conditions

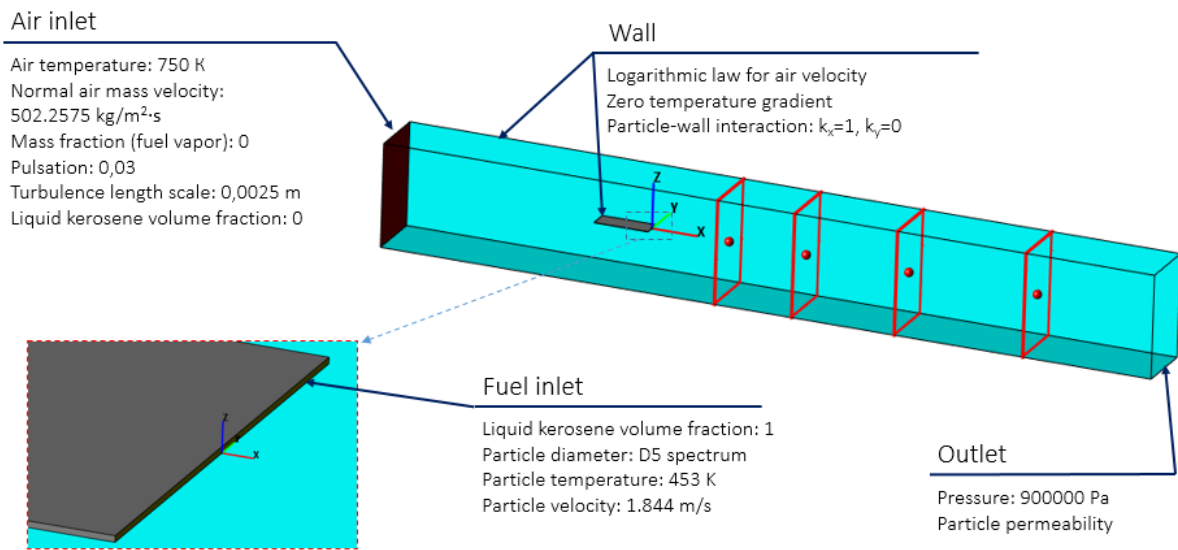


Figure 14. The computational domain and boundary conditions in the 3D problem formulation

The choice of boundary condition is determined by the tangent and normal components (k_x and k_y , respectively) of the particle momentum recovery coefficient after collision with the wall. For example, in the case of a perfectly elastic rebound conserving velocity tangential component, $k_x = 1, k_y = 1$; for a perfectly inelastic rebound conserving velocity tangential component, $k_x = 1, k_y = 0$; in case of sticking, $k_x = 0, k_y = 0$. In this study, particle interaction with the wall is defined as “perfectly inelastic rebound conserving velocity tangential component”. The adaptive grid, built for the three-dimensional problem statement, contained 3.96 million cells. Figure 15 shows the distributions of the kerosene volume fraction (top) and the droplet diameter (bottom). Figure 16 shows the distributions of the kerosene vapor mass fraction (top) and the air temperature (bottom).

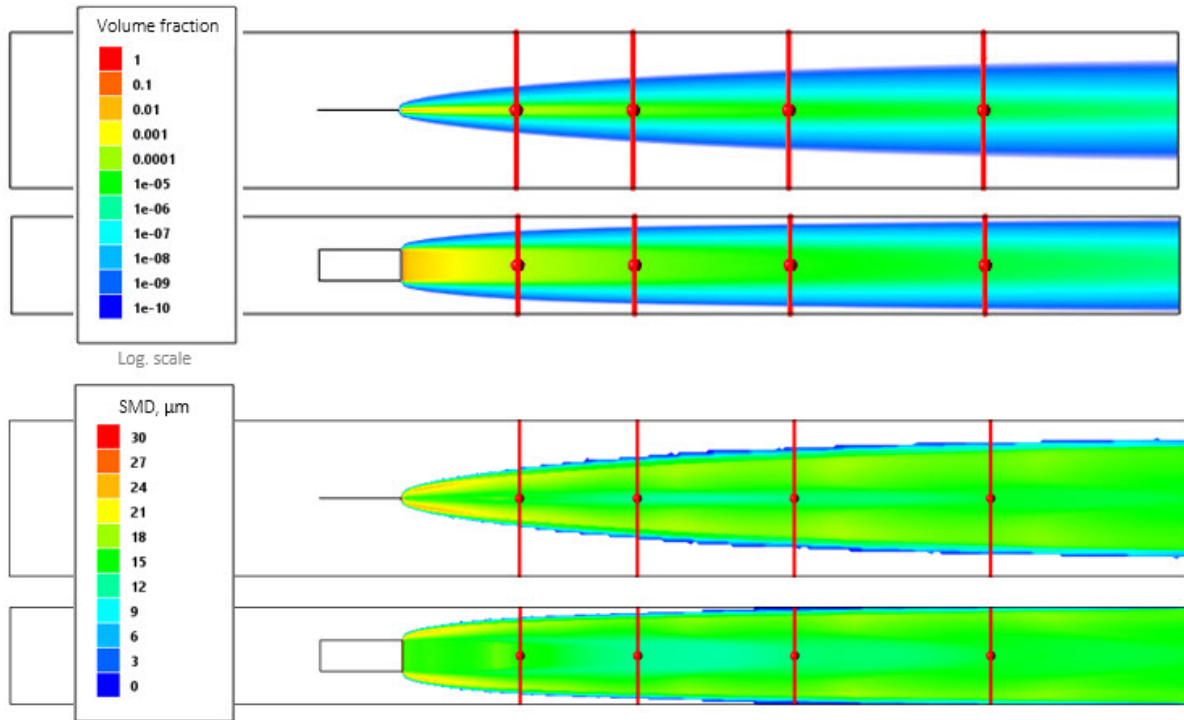


Figure 15. Liquid kerosene volume fraction (top) and SMD (bottom) distributions

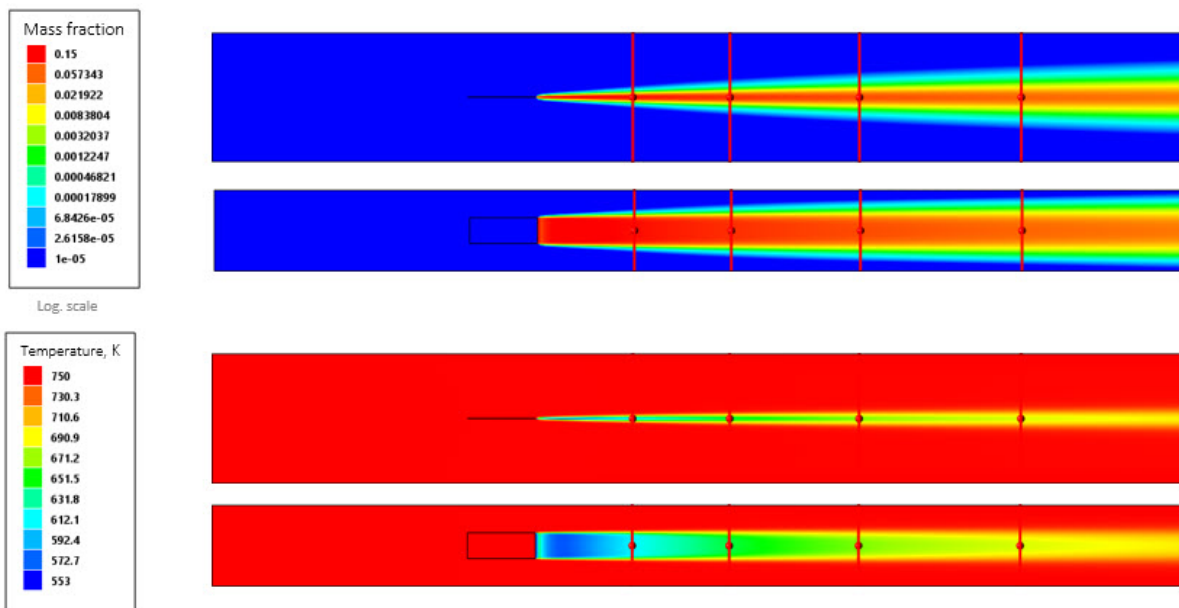


Figure 16. Kerosene vapor mass fraction (top) and air temperature (bottom) distributions

A comparison of the control parameters calculated in the three-dimensional problem statement with experimental data is shown in Fig. 17.

The resources of the Moscow State University (MSU) supercomputer complex allowed for the optimization of the time required to run the required series of test calculations and to speed up the calculation model debugging process and program validation.

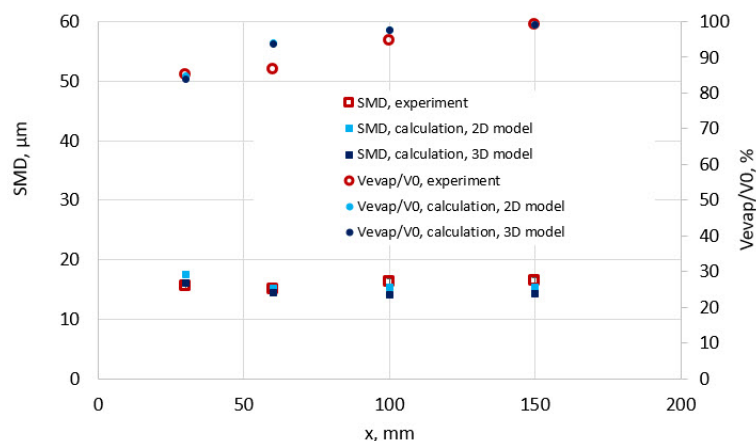


Figure 17. Calculation results on the 3D problem statement

Conclusion

A study of kerosene evaporation in a premix duct for gas turbine combustion chambers at high pressure was carried out in the FlowVision software package based on the experimental data available in literature. Fuel droplet motion and evaporation in the airflow are modeled using the Eulerian approach to continuous- and dispersed- phase interaction. There was a study of the influence on the solution of model parameters such as the computational grid, the atomizer shape, the fuel inlet boundary conditions in terms of the velocity and droplet size, and the inlet air turbulence. In particular, it is found that

- in the modeled scenario of fuel supply in the form of droplets, the atomizer shape has negligible effect on the calculated control values;
- change in the droplet velocity at the inlet from 2 m/s to 10 m/s (in accordance with available data from other published computational studies) affects the results only in the control section closest to the atomizer, where, according to experimental data, an overestimated evaporation rate is observed;
- simulation results significantly depend on the size of fuel droplets at the inlet. It is possible to obtain a correct distribution of control parameters only for a specific droplet size spectrum, which allows to refine results by taking into account the change in droplet acceleration due to flow, the rate of their heating and evaporation depending on droplet diameter and the initial spectrum (as selected based on the cold experiment data);
- inlet air turbulence parameters affect the jet spray width. An increase in the incoming flow pulsations from 3% to 10% achieves an up to 2x increase in the profile width, which contains 90% of the measured volumetric fuel consumption, matching experimentally achieved values.

The evaporation rate and droplet Sauter mean diameter obtained in the selected observed duct sections as a result of the simulation deviate from their corresponding experimentally obtained values by 9% and 12%, respectively, for the basic calculation mode, taking into account the existing uncertainties of the initial data and the assumptions made. Based on a series of calculations for different experimental conditions, it is shown that for the constructed computational model the correct change in fuel evaporation rate with variations in temperature and air pressure is obtained.

Acknowledgements

The authors thank the MSU Research Center and personally V. V. Voevodin for the opportunity to use the Lomonosov-2 supercomputer to obtain the results presented in this article.

This paper is distributed under the terms of the Creative Commons Attribution-Non Commercial 3.0 License which permits non-commercial use, reproduction and distribution of the work without further permission provided the original work is properly cited.

References

1. FlowVision 3.13.03: Users guide. https://flowvision.ru/webhelp/fvru_31303 (2023), accessed: 2023-10-05
2. Aksenov, A.: FlowVision: Industrial computational fluid dynamics. *Computer Research and Modeling* 9(1), 5–20 (2017). <https://doi.org/10.20537/2076-7633-2017-9-5-20>
3. Aksenov, A., Zhlukto, S., Kashirin, V., *et al.*: Numerical modeling of raw atomization and vaporization by flow of heat carrier gas in furnace technical carbon production into FlowVision. *Computer Research and Modeling* 15(4), 921–939 (2023). <https://doi.org/10.20537/2076-7633-2023-15-4-921-939>
4. Aksenov, A., Zhlukto, S., Kashirin, V., *et al.*: Numerical modelling of raw materials atomization and vaporization in a heat carrier gas flow in technical carbon production based on the Euler approach. *E3S Web Conf.* 459, 04019 (2023). <https://doi.org/10.1051/e3sconf/202345904019>
5. Aksenov, A., Zhlukto, S., Platov, S.: Numerical simulation of transition at hull of a ship in FlowVision software. *Ship-building* 4, 58–60 (2013)
6. Brandt, M., Gugel, K., Hassa, C.: Experimental investigation of the liquid fuel evaporation in a premix duct for lean premixed and prevaporized combustion. *Journal of Engineering for Gas Turbines and Power* 119, 815–821 (1997). <https://doi.org/10.1115/1.2817059>
7. Brandt, M., Rachner, M., Schmitz, G.: An experimental and numerical study of kerosene spray evaporation in a premix duct for gas turbine combustors at high pressure. *Combustion Science and Technology* 138:1-6, 313–348 (1998). <https://doi.org/10.1080/00102209808952074>
8. Brinckman, K., Hosangadi, A., Ahuja, V., *et al.*: A CFD Methodology for Liquid Jet Breakup and Vaporization Predictions in Compressible Flows. 46th AIAA Aerospace Sciences Meeting and Exhibit (2008). <https://doi.org/10.2514/6.2008-1023>
9. Hoyas, S., Gil, A., Momp-Laborda, J., Khuong-Anh, D.: A large-eddy simulation of diesel-like gas jets. *Int. J. Vehicle Systems Modelling and Testing* 6(3/4), 268–282 (2011). <https://doi.org/10.1504/IJVSMT.2011.044229>
10. Irannejad, A., Banaeizadeh, A., Jaber, F.: Large eddy simulation of turbulent spray combustion. *Combustion and Flame* 162(2), 431–450 (2015). <https://doi.org/10.1016/j.combustflame.2014.07.029>

11. Keser, R., Battistoni, M., Im, H., Jasak, H.: An eulerian multi-fluid model for high-speed evaporating sprays. *Processes* 9(6), 941 (2021). <https://doi.org/10.3390/pr9060941>
12. Luo, K., Pitsch, H., Pai, M., Desjardins, O.: Direct numerical simulations and analysis of three-dimensional n-heptane spray flames in a model swirl combustor. In: *Proceedings of the Combustion Institute*. vol. 33, pp. 2143–2152 (2011). <https://doi.org/10.1016/j.proci.2010.06.077>
13. Malaguti, S., Cantore, G., Fontanesi, S., *et al.*: CFD Investigation of Wall Wetting in a GDI Engine under Low Temperature Cranking Operations. SAE Technical Paper 2009-01-0704 (2009). <https://doi.org/10.4271/2009-01-0704>
14. Perini, F., Mattarelli, E.: A large-eddy simulation of diesel-like gas jets. *International Journal of Engine Research* 12(4), 311–335 (2011). <https://doi.org/10.1177/1468087411401285>
15. Rachner, M.: Die stoffeigenschaften von kerosin Jet A-I. DLR-Mitteilungen 98-01 (1) (1998)
16. Rachner, M., Brandt, M., Eickhoff, H., *et al.*: A numerical and experimental study of fuel evaporation and mixing for lean premixed combustion at high pressure. *Symposium (International) on Combustion* 26(2), 2741–2748 (1996). [https://doi.org/10.1016/S0082-0784\(96\)80111-1](https://doi.org/10.1016/S0082-0784(96)80111-1)
17. Schmehl, R., Klose, G., Maier, G., Wittig, S.: Efficient numerical calculation of evaporating sprays in combustion chamber flows. RTO AVT Symposium on “Gas Turbine Engine Combustion, Emissions and Alternative Fuels” (1998)
18. Som, S., Aggarwal, S.: Effects of primary breakup modeling on spray and combustion characteristics of compression ignition engines. *Combustion and Flame* 157(6), 1179–1193 (2010). <https://doi.org/10.1016/j.combustflame.2010.02.018>
19. Som, S., Ramirez, A., Longman, D., Aggarwal, S.: Effect of nozzle orifice geometry on spray, combustion, and emission characteristics under diesel engine conditions. *Fuel* 90(3), 1267–1276 (2011). <https://doi.org/10.1016/j.fuel.2010.10.048>
20. Sorokin, K., Zhluktov, S., Aksenov, A.: On the implementation of the Euler approach to modeling polydisperse media in the FlowVision software package. *Thermophysics and Physical Hydrodynamics. Collection of abstracts of the VI All-Russian scientific conference with elements of the school of young scientists* p. 201 (2021)
21. Tonini, S., Gavaises, M., Theodorakakos, A.: Modelling of high-pressure dense diesel sprays with adaptive local grid refinement. *International Journal of Heat and Fluid Flow* 29(2), 427–448 (2008). <https://doi.org/10.1016/j.ijheatfluidflow.2007.11.009>
22. Tonini, S., Gavaises, M., Theodorakakos, A., Cossali, G.: Numerical investigation of a multiple injection strategy on the development of high-pressure diesel sprays. In: *Proceedings of the Institution of Mechanical Engineers, Part D: Journal of Automobile Engineering*. vol. 224, pp. 125–141 (2010). <https://doi.org/10.1243/09544070JAUTO1083>
23. Zhluktov, S., Aksenov, A., Karasev, A.: Simulation of a bypass laminar-turbulent transition in the framework of the k- ε -approach. *Computer Research and Modeling* 6(6), 879–888 (2014)